Water Research 140 (2018) 354–363

Contents lists available at ScienceDirect

Water Research

journal homepage: www.elsevier.com/locate/watres

Quantitative structure–activity relationship for the oxidation of aromatic organic contaminants in water by TAML/H_2O_2

Hanrui Su [a], Chunyang Yu [b], Yongfeng Zhou [b], Lidong Gong [c], Qilin Li [d], Pedro J.J. Alvarez [d], Mingce Long [a, e, *]

[a] School of Environmental Science and Engineering, Shanghai Jiao Tong University, Shanghai 200240, China
[b] School of Chemistry and Chemical Engineering, Shanghai Jiao Tong University, Shanghai 200240, China
[c] School of Chemistry and Chemical Engineering, Liaoning Normal University, Dalian 116029, China
[d] Department of Civil and Environmental Engineering, Rice University, Houston, TX 77005, United States
[e] Key Laboratory for Thin Film and Microfabrication Technology (Ministry of Education), Shanghai Jiao Tong University, Shanghai 200240, China

ARTICLE INFO

Article history:
Received 30 January 2018
Received in revised form
23 April 2018
Accepted 27 April 2018
Available online 2 May 2018

Keywords:
Quantitative structure–activity relationship
TAML
Oxidation
Aromatic organic contaminants

ABSTRACT

Tetra-amido macrocyclic ligand (TAML) activator is a functional analog of peroxidase enzymes, which activates hydrogen peroxide (H_2O_2) to form high valence iron-oxo complexes that selectively degrade persistent aromatic organic contaminants (ACs) in water. Here, we develop quantitative structure–activity relationship (QSAR) models based on measured pseudo first-order kinetic rate coefficients (k_{obs}) of 29 ACs (e.g., phenols and pharmaceuticals) oxidized by TAML/H_2O_2 at neutral and basic pH values to gain mechanistic insight on the selectivity and pH dependence of TAML/H_2O_2 systems. These QSAR models infer that electron donating ability (E_{HOMO}) is the most important AC characteristic for TAML/H_2O_2 oxidation, pointing to a rate-limiting single-electron transfer (SET) mechanism. Oxidation rates at pH 7 also depend on AC reactive indices such as f_{min}^{-} and qH^{+}, which respectively represent propensity for electrophilic attack and the most positive net atomic charge on hydrogen atoms. At pH 10, TAML/H_2O_2 is more reactive towards ACs with a lower hydrogen to carbon atoms ratio (#H:C), suggesting the significance of hydrogen atom abstraction. In addition, ln k_{obs} of 14 monosubstituted phenols is negatively correlated with Hammett constants (σ) and exhibits similar sensitivity to substituent effects as horseradish peroxidase. Although accurately predicting degradation rates of specific ACs in complex wastewater matrices could be difficult, these QSAR models are statistically robust and help predict both relative degradability and reaction mechanism for TAML/H_2O_2-based treatment processes.

1. Introduction

A variety of natural and synthetic refractory aromatic organic contaminants (ACs) such as phenolic compounds and pharmaceuticals break through wastewater treatment plants and are released into natural water systems, which can impact aquatic ecosystems and human health (Pal et al., 2010). This has increased interest in tertiary wastewater treatment. Physical adsorption/filtration (granular activated carbon and membrane separation) and advanced oxidation processes (AOPs, e.g., ozonation, Fenton oxidation and persulfate-based oxidation) have been considered to remove trace ACs, but the high financial and energy costs have limited their applications (Zheng et al., 2017; Hu et al., 2017; Wang et al., 2017b) .

The tetra-amido macrocyclic ligand catalyst (TAML, Fig. 1), which is as a functional analog of peroxidase enzyme, is a simple and potentially effective green alternative to AOPs (Gupta et al., 2002). TAML activates hydrogen peroxide (H_2O_2) to form a high valence iron-oxo complex that is very reactive and more selective for oxidation of ACs than AOP-generated, easily-scavenged free radicals in complex wastewater matrices (Chanda et al., 2006a). The toxicity of contaminated water was reported to dramatically decrease after treatment with TAML/H_2O_2, and residual traces of TAML had no adverse effects on fish or microorganisms (Ellis et al., 2010). Additionally, TAML can be used at very low (nM to low μM) concentrations (e.g., 1 kg of catalysts could treat 20,000 tons of water (Shappell et al., 2008)) and offers high efficiency for near-

* Corresponding author. School of Environmental Science and Engineering, Shanghai Jiao Tong University, Shanghai 200240, China.
E-mail address: long_mc@sjtu.edu.cn (M. Long).

https://doi.org/10.1016/j.watres.2018.04.062
0043-1354/

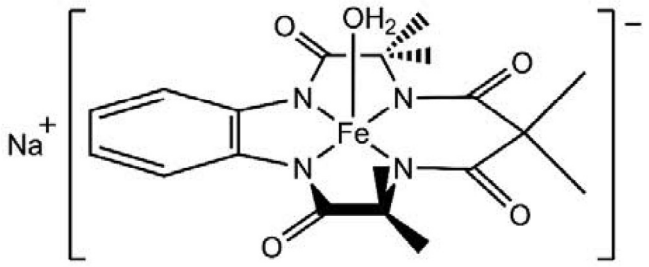

Fig. 1. Molecule structure of prototype TAML activator used in this study.

stoichiometric hydrogen peroxide utilization (Tang et al., 2016). Accordingly, TAML has been used to degrade a wide variety of ACs in wastewater, including dyes (Chahbane et al., 2007; Chanda et al., 2006a; Ellis et al., 2009), estrogenic compounds (Chen et al., 2012; Onundi et al., 2017; Shappell et al., 2008), persistent chloro- (Gupta et al., 2002), nitro- (Kundu et al., 2015) and bromo- (Wang et al., 2017a) phenols, thiophosphate pesticides (Chanda et al., 2006b), molluscicides (Tang et al., 2016), and drugs (Shen et al., 2011).

TAML activates H_2O_2 to form oxidized TAML, which in turn oxidizes the AC molecule and restores itself to TAML (Scheme 1). The initial rates of AC oxidation are given by Eq. (1), in which $[TAML]_0$ is the total concentration of TAML catalyst, k_I is the first-order rate constant for TAML oxidation, k_{-I} is the rate constant for the reversal reaction, and k_{II} is the rate constant for AC oxidation (Chahbane et al., 2007). If $k_I[H_2O_2] \gg k_{II}[AC]$ and k_{-I} is negligible, Eq. (1) simplifies to Eq. (2).

$$-\frac{d[AC]}{dt} = \frac{k_I k_{II}[H_2O_2][AC]}{k_{-I} + k_I[H_2O_2] + k_{II}[AC]}[TAML]_0 \quad (1)$$

$$-\frac{d[AC]}{dt} = k_{II}[AC][TAML]_0 = k_{obs}[AC] \quad (2)$$

The reactivity of oxidized TAML towards different ACs is highly variable (Table S1), depending on the structures of both TAML and the target ACs. Previously, it was shown that the electron-withdrawing groups on the aromatic ring of TAML enhance both k_I and k_{II} (Chahbane et al., 2007). However, little is known about how AC structure affects treatment efficiency. Furthermore, the speciation of oxidized TAML changes with pH (Ghosh et al., 2008), which in turn affects both reaction rates and products distribution (Chanda et al., 2006b; Onundi et al., 2017). Therefore, TAML-based treatment process optimization and reliability enhancement requires improved understanding and accurate prediction of how AC structure and solution pH affect reaction mechanisms and kinetics.

Quantitative structure-activity relationship (QSAR) models are powerful tools to correlate degradation rates and physicochemical properties of molecules. Numerous successful QSAR models have been used to predict reaction rate constants for organic contaminants oxidation by ozone (O_3) (Sudhakaran and Amy, 2013), chlorine dioxide (ClO_2) (Lee and von Gunten, 2012), UV (Luo et al., 2018a), UV/H_2O_2 (Xiao et al., 2016), hexavalent ferrate (Fe (VI)) (Ye et al., 2017), and free radicals such as •OH (Borhani et al., 2016; Luo et al., 2017a; Xiao et al., 2017) and $SO_4^{\bullet-}$ (Xiao et al., 2015; Luo et al., 2018b). For example, the second-order rate constant for the reaction of horseradish peroxidase (HRP) with 32 phenolic or aniline compounds was positively correlated with Hammett sigma constants (Na and Lee, 2017). Furthermore, the second-order rate constants for the oxidation of 34 aromatic compounds by Fe (VI), which is another high valence iron-oxo compound, was negatively correlated with ionization potential (IP) (Ye et al., 2017); this implies that SET was the rate-limiting first step. These examples demonstrate the potential of QSAR models to predict rate constants of diverse ACs oxidation reactions and to inform rate-limiting mechanisms.

In this work, we develop QSAR models to predict reactivity and elucidate the reaction mechanism and selectivity of TAML/H_2O_2-based oxidative treatment, based on rate constants measured for 29 ACs at pH 7 and pH 10. Representative molecule descriptors (42 in total) including constitutional, geometrical, physicochemical, quantum chemical, and electrostatic descriptors, were considered to develop models by stepwise multiple linear regression (MLR). Correlation analyses, internal and external validation, and applicability domain assessment were also conducted to assess the statistical robustness of these models and to gain mechanistic insight on rate-limiting reactions.

$$TAML + H_2O_2 \underset{k_{-I}}{\overset{k_I}{\rightleftarrows}} \text{Oxidized TAML}$$

$$\text{Oxidized TAML} + AC \xrightarrow{k_{II}} TAML + \text{Primary product}$$

$$\text{Primary product} \xrightarrow{fast} \rightarrow\rightarrow \text{Final product(s)}$$

Scheme 1. General mechanism of TAML/H_2O_2 systems.

2. Material and methods

2.1. Chemicals

Sodium salt of TAML was obtained from GreenOx Catalysts, Inc. and dissolved in deionized water at 1×10^{-4} M. All standards for the organic compounds, H_2O_2 (30 wt%), NaH_2PO_4, and Na_2HPO_4 were analytical grade and purchased from Sinopharm Chemical Reagent Co., Ltd. Methanol of high performance liquid chromatography (HPLC) grade was obtained from Thermo Fisher Scientific. The stock solutions of ACs were prepared with phosphate buffer solution or methanol depended on the solubility.

2.2. Kinetic experiments

The batch experiments were conducted according to the following procedures. Each experiment was performed with 25 ml reaction solution in a 50 mL flask kept in a 25 °C water bath. The oxidation reaction was initiated by adding an aliquot of H_2O_2 (4×10^{-3} M) to the phosphate buffer solution (5×10^{-2} M) containing the standard AC (1×10^{-4} M) and TAML catalyst (1×10^{-6} M). At predetermined intervals, 0.5 ml of sample was withdrawn, immediately added into a HPLC vial, and acidified to pH 2 with 0.1 M HCl to terminate the catalytic reaction. Specifically, demetalation (i.e., loss of the iron metal) of TAML results in irreversible activity loss at acidic pH, with cleavage of the Fe-N bond in TAML occurring at pH lower than 4 (Ghosh et al., 2003). Considering the pH-dependent performance of TAML oxidation, experiments were conducted at pH 7 and 10, which represent pH values commonly encountered in wastewater treatment and the optimal pH for TAML oxidation, respectively. The concentrations of ACs were quantitatively determined by HPLC (LC-2010AHT, Shimadzu) equipped with a C-18 column (Shim-pack GIST C18) and an UV-vis detector (SPD-20AV). Detailed HPLC analytical conditions including

mobile phase, flow rate, and the detection wavelength are listed in Table S2. All experiments were conducted in triplicate.

Under our experimental conditions with excess H_2O_2 over ACs and TAML concentrations, the batch systems exhibited pseudo-first-order kinetics. Apparent first-order degradation rate constants (k_{obs}, min^{-1}) were obtained from initial rates of all catalytic processes by linear regression of natural logarithm of the AC concentrations versus time (Eq. (3)):

$$\ln([AC]_0/[AC]_t) = k_{obs} \times t \quad (3)$$

where $[AC]_0$ and $[AC]_t$ are the respective concentrations of AC at initial and reaction time (t) (Figs. S1 and S2).

2.3. Molecular descriptors

To identify molecular descriptors that impact ACs reactivity, a total number of 42 representative molecular descriptors were selected based on previous study (Table S3) (Xiao et al., 2015; Zhu et al., 2015; Radian et al., 2015), including constitutional (#C, #H, #O, #N, #X, #OH, #Acid, #H:C, #O:C, number of aromatic bonds (#AB), number of atoms in the largest pi system (#Pi), double bond equivalence (DBE), mean oxidation number of carbon (MOC), hydrogen bond donor count (HD), hydrogen bond acceptor count (HA), rotatable bond count (RB)), geometrical (molecular complexity (CPLX), topological polar surface area (TPSA), molar volume (V)), physicochemical (pKa, logP, ClogP, ClogS), quantum chemical (E_{HOMO}, E_{LUMO}, $E_{LUMO} - E_{HOMO}$ (E_{gap}), IP, electron affinity (EA), hardness (η), softness (S)), and electrostatic (electronegativity (ζ), electrophilicity index (ω), dipole moment (μ), average polarizability (α), Fukui indices (f^+_{min},f^-_{min},f^0_{min},f^+_{max},f^-_{max}, and f^0_{max}), the most positive net atomic charge on hydrogen atoms (qH^+), the most negative net atomic charge on carbon atoms (qC^-)) descriptors.

The quantum chemical and electrostatic descriptors were calculated based on density functional theory (DFT). The conformational search for the global minimum structure of ACs was first performed using the Merck Molecular Force Field (MMFF94) in the Tinker software (Version 5.1.9) (Ponder, 2004). Then, the resulting conformations with minimum energy were calculated using Becke's three parameter hybrid functional (B3LYP) coupled with the economical 6−31 + G(d,p) basis set provided by the Gaussian 09 W for further geometry optimizations (Borhani et al., 2016; Yang et al., 2016). There was no imaginary vibrational frequency for the optimized geometries, indicating they are at a minimum on the potential energy surface.

The net atomic charge values for each compound were obtained from the natural population analysis (NPA) procedure. The condensed Fukui functions are found by taking the finite difference approximations from NPA of atoms in molecules, depending on the electron-transfer direction (Yang and Mortier, 1986):

$$f_i^+ = q_i(N+1) - q_i(N) \quad (4)$$

$$f_i^- = q_i(N) - q_i(N-1) \quad (5)$$

$$f_i^0 = \frac{1}{2}[q_i(N+1) - q_i(N-1)] \quad (6)$$

where $q_i(N)$, $q_i(N+1)$, $q_i(N-1)$ are electronic population of atoms i in neutral, anionic, and cationic molecule, respectively. f_i^+, f_i^-, f_i^0 indices were defined to describe nucleophilic, electrophilic, and radical attack. Further, the minimum (f^+_{min},f^-_{min},f^0_{min}) and maximum (f^+_{max}, f^-_{max}, f^0_{max}) condensed Fukui indices were collected as descriptors. All the calculated results of quantum chemical and electrostatic descriptors were listed in Table S4.

2.4. QSAR analyses

All rate constants were randomly divided into the training set (22 ACs) for developing the QSAR models and test set (7 ACs) for validating the models. A stepwise MLR was used to develop the predictive model, by correlating $\ln k_{obs}$ and all descriptors of ACs compounds.

Next, various strategies were adopted for validation of QSAR models. Statistics such as coefficient of determination R^2, F value, significance level p, and variance inflation factor (VIF) were used to assess internal performance. Leave-one-out (LOO) method was used for cross-validation. For external validation, Q^2_{ext} and average absolute model bias (AMB) were used for estimating the predictive capacity of the QSAR model, which were calculated as Eq. (7) and Eq. (8) (Xiao et al., 2015):

$$Q^2_{ext} = 1 - \frac{\sum_{i=1}^{test}\left(y_i - \hat{y}_i\right)^2}{\sum_{i=1}^{test}\left(y_i - \overline{y}_i\right)^2} \quad (7)$$

$$AMB = \frac{\sum_1^n ABS\left(\frac{\hat{y}_i}{y_i}\right)}{n} \quad (8)$$

where y_i and $\hat{y}_i$ are the observed and predicted $\ln k_{obs}$ values, respectively, for compound i; $\overline{y_i}$ is average value for the training set; n is the number of training set.

Finally, the applicability domain was characterized by a Williams plot (i.e., the standardized residuals vs. leverage). The standardized residuals (δ) and the leverage (h) were calculated using Eq. (9) and Eq. (10):

$$\delta = \frac{y_i - \hat{y}_i}{\sqrt{\sum_{i=1}^n\left(y_i - \hat{y}_i\right)^2 \Big/ (n - P - 1)}} \quad (9)$$

$$h = x_i^T\left(X^T X\right)^{-1} x_i \quad (10)$$

where P is the number of descriptors included in the model; x_i is the row vector of the descriptors of compound i; X is descriptor matrix for the training set. The warning leverage was defined as $h^* = 3(P+1)/n$. Predictions for new compounds lying within the applicability domain are supposed to be reliable (Tropsha et al., 2003). Statistical analyses were performed using the IBM SPSS Statistics software (Version 24).

3. Results and discussion

3.1. Model development

Table 1 summarizes the measured rate constants of TAML/H_2O_2 oxidation for 29 ACs at pH 7 and pH 10. Reaction kinetics followed pseudo first-order (Figs. S1 and S2), with k_{obs} values (at pH 7) ranging over two orders of magnitude from 4.0×10^{-4} min^{-1} (for metronidazole) to 6.9×10^{-2} min^{-1} (for 4-aminophenol). The k_{obs} values were transformed into natural logarithm units ($\ln k_{obs}$) to

Table 1
The rate constants of all 29 ACs oxidized by TAML/H_2O_2 at pH 7 and pH 10.

Organic compounds	k_{obs} (min^{-1})	$\ln k_{obs}$	$\ln k_{pred}$	k_{obs} (min^{-1})	$\ln k_{obs}$	$\ln k_{pred}$
	pH 7			pH 10		
Training set						
Monosubstituted phenols						
Phenol	$(3.08 \pm 0.19) \times 10^{-2}$	−3.48	−3.75	4.28 ± 0.09	1.46	−0.37
Catechol	$(2.17 \pm 0.14) \times 10^{-2}$	−3.83	−3.13	1.07 ± 0.06	0.07	1.05
Resorcinol	$(2.70 \pm 0.78) \times 10^{-3}$	−5.91	−4.80	0.18 ± 0.006	−1.72	0.05
p-Cresol	$(3.68 \pm 0.11) \times 10^{-2}$	−3.30	−4.78	4.67 ± 0.13	1.54	−0.45
4-Aminophenol	$(6.91 \pm 0.16) \times 10^{-2}$	−2.67	−0.99	7.23 ± 0.53	1.98	3.03
4-Nitrophenol	$(5.00 \pm 2.83) \times 10^{-4}$	−7.60	−6.93	$(6.70 \pm 0.78) \times 10^{-3}$	−5.01	−2.88
4-Acetamidophenol	$(3.76 \pm 0.11) \times 10^{-2}$	−3.28	−3.44	6.91 ± 0.05	1.93	0.60
4-Chlorophenol	$(5.70 \pm 0.28) \times 10^{-2}$	−2.86	−3.42	8.08 ± 0.42	2.09	0.59
4-Bromophenol	$(5.60 \pm 0.29) \times 10^{-2}$	−2.88	−3.37	6.46 ± 0.18	1.87	0.75
Guaiacol	$(1.91 \pm 0.06) \times 10^{-2}$	−3.96	−3.92	4.67 ± 0.04	1.54	0.54
Salicylaldehyde	$(6.30 \pm 0.16) \times 10^{-3}$	−5.07	−5.81	0.12 ± 0.002	−2.09	−1.39
Pharmaceuticals						
Sulfanilamide	$(9.50 \pm 0.04) \times 10^{-3}$	−4.66	−5.47	$(3.56 \pm 0.18) \times 10^{-2}$	−3.34	−2.75
Ibuprofen	$(9.00 \pm 2.47) \times 10^{-4}$	−7.01	−5.47	$(3.20 \pm 0.28) \times 10^{-3}$	−5.74	−4.42
Metronidazole	$(4.00 \pm 2.76) \times 10^{-4}$	−7.82	−7.02	$(3.00 \pm 0.71) \times 10^{-4}$	−8.11	−7.83
Amoxicillin	$(2.26 \pm 0.11) \times 10^{-2}$	−3.79	−4.73	2.49 ± 0.12	0.91	−2.62
Diphenhydramine	$(6.00 \pm 1.84) \times 10^{-4}$	−7.42	−7.29	$(3.21 \pm 0.22) \times 10^{-2}$	−3.44	−0.91
Tetracycline	$(1.61 \pm 0.09) \times 10^{-2}$	−4.13	−3.93	1.93 ± 0.07	0.66	0.83
Chlortetracycline	$(3.04 \pm 0.18) \times 10^{-2}$	−3.49	−3.83	2.78 ± 0.04	1.02	1.33
Other organics						
2,3-Dihydroxybenzoic acid	$(2.91 \pm 0.08) \times 10^{-2}$	−3.54	−4.41	3.95 ± 0.06	1.37	0.41
2,5-Dihydroxybenzoic acid	$(3.54 \pm 0.20) \times 10^{-2}$	−3.34	−4.23	1.89 ± 0.02	0.63	1.17
4,4′-Biphenol	$(3.38 \pm 0.17) \times 10^{-2}$	−3.39	−3.55	3.06 ± 0.01	1.12	3.71
Benzoic acid	$(5.00 \pm 1.34) \times 10^{-4}$	−7.60	−6.81	$(1.50 \pm 0.28) \times 10^{-3}$	−6.50	−3.50
Test set						
Monosubstituted phenols						
Hydroquinone	$(2.72 \pm 0.11) \times 10^{-2}$	−3.60	−2.19	2.93 ± 0.02	1.08	1.57
4-Methoxyphenol	$(3.22 \pm 0.17) \times 10^{-2}$	−3.44	−3.75	7.05 ± 0.23	1.95	1.00
4-Hydroxybenzaldehyde	$(1.50 \pm 0.14) \times 10^{-3}$	−6.50	−6.09	$(8.20 \pm 0.21) \times 10^{-3}$	−4.80	−1.40
Pharmaceutical						
Oxytetracycline	$(1.66 \pm 0.13) \times 10^{-2}$	−4.10	−3.81	1.85 ± 0.07	0.62	1.34
Other organics						
3,4,5-Trihydroxybenzoic acid	$(2.72 \pm 0.16) \times 10^{-2}$	−3.60	−4.69	1.67 ± 0.03	0.51	0.18
Bisphenol A	$(6.72 \pm 0.11) \times 10^{-2}$	−2.70	−3.78	4.47 ± 0.19	1.50	0.64
Furfuryl alcohol	$(2.30 \pm 0.52) \times 10^{-3}$	−6.07	−5.09	$(4.06 \pm 0.10) \times 10^{-2}$	−3.20	−1.10

reduce the span of the data.

The QSAR models were developed with the $\ln k_{obs}$ in the training set ($n = 22$) and all 42 molecular descriptors. A correlation analysis between the $\ln k_{obs}$ and selected individual descriptors was performed to assess the interrelationship strengths. The correlation coefficients (r) and the statistical significances were listed in Table S5. Among the descriptors correlated with $\ln k_{obs}$ at pH 7, E_{HOMO} ($r = 0.69$), IP ($r = -0.64$), ζ ($r = -0.56$) and f_{min}^{-} ($r = 0.53$) are highly significant ($p < 0.01$). The results at pH 10 are similar, and the order of correlation coefficients ($p < 0.05$) is E_{HOMO} ($r = 0.74$) > IP ($r = -0.70$) > ζ ($r = -0.60$) > f_{min}^{-} ($r = 0.47$) > #OH ($r = 0.37$). However, E_{HOMO} is highly negatively correlated with IP ($r = -0.95$, $p < 0.01$), suggesting the collinearity between them. Interestingly, strongly negative correlation has also been found in E_{LUMO} with EA and ω, proving that the calculated E_{LUMO} can be used for estimating these two descriptors (Zhan et al., 2003). Moreover, the $\ln k_{obs}$ values obtained at pHs 7 and 10 have a correlation coefficient of 0.95 ($p < 0.01$), indicating TAML/H_2O_2 systems may have similar reactive preference toward these ACs at different pHs.

To avoid missing descriptors with low correlation but high importance, all 42 descriptors were selected for stepwise MLR analysis, and 6 models were listed in Table S6. Although the coefficient of determination R^2 increases as the number of variables increases, the p value of the last model for pH 10 is larger than 0.05, thus #AB was excluded from the model. The models for pH 7 and pH 10 were obtained as Eq. (11) and Eq. (12), respectively.

$$\ln k_{obs} = 2.32 + 1.95 \times E_{HOMO} + 11.6 \times qH^{+} + 27.9 \times f_{min}^{-} \quad (pH = 7) \tag{11}$$

$n = 22$, $R^2 = 0.762$, $F = 18.1$, $p < 0.01$, VIF < 1.2, $Q_{LOO}^2 = 0.627$, $Q_{ext}^2 = 0.566$

$$\ln k_{obs} = 35.6 + 4.53 \times E_{HOMO} - 7.42 \times \#H : C \quad (pH = 10) \tag{12}$$

$n = 22$, $R^2 = 0.747$, $F = 26.6$, $p < 0.01$, VIF < 1.1, $Q_{LOO}^2 = 0.626$, $Q_{ext}^2 = 0.619$.

The respective coefficients of determination R^2 for $\ln k_{obs}$ at pH 7 and pH 10 are 0.762 and 0.747, respectively, which suggest that these QSAR models reasonably fitted well with the training set. The reasonable F values (18.1 and 26.6) and low p level (<0.01) indicate these $\ln k_{obs}$ values are unlikely distributed under the null hypothesis, which would be rejected. Further, the VIF values are less than 1.2, indicating no potential collinearities among the descriptors included in the models. The values of R^2 (>0.6), F (>15), p (<0.05), and VIF (<10) all meet the minimum statistical robustness criteria (Tropsha et al., 2003).

For internal validation ($n = 22$), both Q_{LOO}^2 values (0.627 and 0.626) are larger than 0.5, corroborating that the models are statistically robust with no obvious over-fitting. The models predict reasonably well the reactivity of the ACs used for external

validation ($n = 7$). The calculated Q^2_{ext} values are 0.566 and 0.619 for pH 7 and 10, respectively. The $AMB_{training}$ is 1.03 and 1.75, and the AMB_{test} is 1.01 and 0.90 for pH 7 and pH 10, respectively. The absolute model bias (100% and 86.2% for pH 7 and pH 10) is within a factor of 0.5–2, confirming the predictive power of the QSAR models. The comparison of measured and predicted ln k_{obs} value is shown in Fig. 2. The 1:1 solid line shows perfect agreement. Among the different families of ACs, the monosubstituted phenols exhibit relatively high lnk_{obs} but the goodness of the fitting is similar for all ACs. Moreover, the probability-probability (P-P) plots show random normal distribution for observed standard residuals, demonstrating the validity of the regression models (Fig. S3).

The Williams plot was used to evaluate the applicability domain of the QSAR models for oxidation of ACs (Fig. 3). The horizontal dash lines are standardized residual outliers (±3) and vertical dash lines are warning leverages ($h^* = 0.545$ and 0.409). As can be seen from Fig. 3, all data points in the training set and the test set fall into applicability domain, indicating the QSAR models are reliable for predicting k_{obs} of ACs by TAML/H_2O_2. Only diphenhydramine has relatively high leverage ($h = 0.499$), but does not exceed h^*. However, the models fit these data reasonably well with small standardized residuals, which improves model stability. No significant difference was found in the applicability domain for different families of ACs, suggesting that the QSAR models are broadly applicable to phenolic compounds, pharmaceuticals, and organic acids.

3.2. Implications of model descriptors

The QSAR models expressed as Eq. (11) and Eq. (12) show that quantum chemical (E_{HOMO}) and electrostatic (f^-_{min}, qH^+) descriptors are directly proportional to lnk_{obs}, whereas constitutional descriptor (#H:C) is inversely proportional to it. The contribution of each variable to Eq. (11) is 44.8% for E_{HOMO}, 27.9% for qH^+, and 27.3% for f^-_{min}, respectively. For Eq. (12), E_{HOMO} and #H:C contributed 63.4% and 36.6% of the variance.

Both models include E_{HOMO}, the energy of the highest occupied molecular orbital, which may be the predominant factor affecting the reactivity of ACs towards TAML/H_2O_2. The experimental lnk_{obs} exhibits a linear trend when correlated with the respective E_{HOMO} (Figs. S4a and S4b). Although the coefficients of determination are relatively low ($R^2 = 0.47$ for pH 7 and $R^2 = 0.55$ for pH 10), the general trends show that reactivity increases with E_{HOMO}. The compounds with higher E_{HOMO} are better electron donors. 4-Aminophenol has the highest E_{HOMO} and hence the strongest ability to donate electrons. The reaction of high valence iron-oxo species with organic compounds is known to be an electrophilic reaction via a SET process (Chahbane et al., 2007). The descriptor E_{HOMO} has frequently been included in other QSAR models for oxidation reactions. For example, Lee et al. (2015) developed a QSAR model for the second-order rate constants of the reaction between O_3 and 112 aromatic micropollutants in aquatic systems. They reported R^2 values of 0.82–1.00 with only E_{HOMO} as a descriptor. Salter-Blanc et al. (2016) built QSAR models for relative rate constants of aromatic amine oxidation by manganese dioxide (MnO_2), and found that E_{HOMO} calculated by different functionals (Hartree–Fock, B3LYP, or M06–2X) and basis sets (6–31G* or 6–311++G(2d,2p)) correlate well with the logarithm of the relative rate constants. In addition to O_3 and mineral oxidants, the rate constants of biocatalysts such as HRP and bovine methemoglobin are also positively correlated with the E_{HOMO} of monosubstituted phenols (Pérez-Prior et al., 2012; Sakurada et al., 1990). These similarities are consistent with the peroxidase-like reaction of TAML/H_2O_2 systems, indicating that the oxidation rate is controlled by the SET from the ACs to the active iron center.

Other quantum chemical descriptors such as E_{gap} and IP have been used to establish QSAR models for organic contaminants oxidation by O_3 (Sudhakaran and Amy, 2013), $SO_4^{\bullet-}$ (Xiao et al., 2015; Luo et al., 2018b) and Fe (VI) (Ye et al., 2017) in aqueous systems. No significant correlation was found between ln k_{obs} and E_{gap}, which is the predominant descriptor affecting oxidation by $SO_4^{\bullet-}$ (Xiao et al., 2015). This suggests that the reactions of TAML/H_2O_2 with the ACs used here are less likely to proceed through the nucleophilic addition pathway. IP is approximately equal to the negative E_{HOMO} (Table S5), but less significant than E_{HOMO} for TAML/H_2O_2 oxidation thus excluded by stepwise MLR.

Fukui indices f^+_i, f^-_i, and f^0_icould quantitatively reflect the respective affinity with nucleophilic attack, electrophilic attack, and radical attack, which may suggest reaction mechanisms. For example, Zhu et al. (2015) measured the rate constants of O_3 with 33 kinds of ACs under acidic conditions, and observed that lnk_{obs} correlates strongly with f^0_{max}, which represented radical attack. For the reaction at pH 7, the correlation between descriptor f^-_{min} and lnk_{obs} is not high but significant ($r = 0.53$, $p < 0.01$). Fig. S4c shows

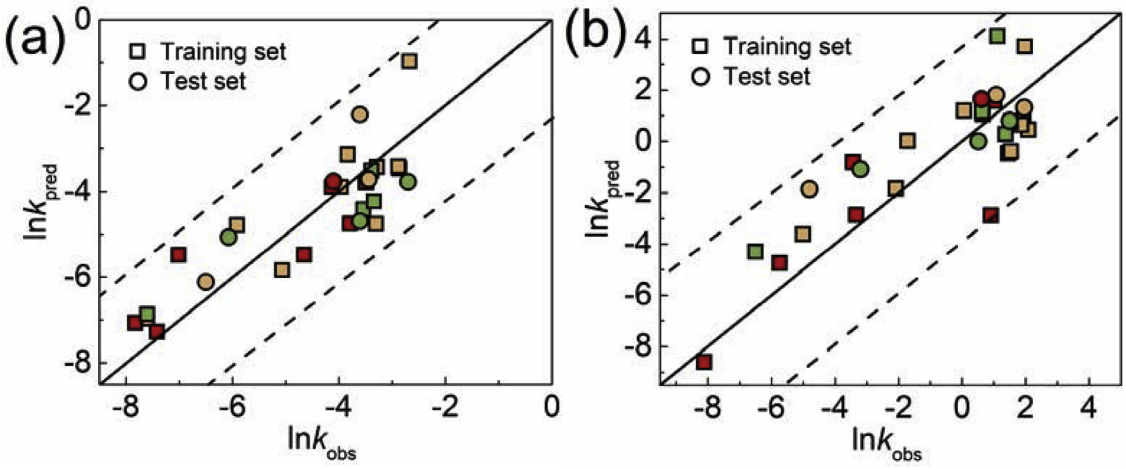

Fig. 2. Plots of the measured and predicted ln k_{obs} for oxidation of ACs by TAML/H_2O_2 at (a) pH 7 and (b) pH 10. Fill colors with orange, red, and green were represented for monosubstituted phenols, pharmaceuticals and other organic compounds, respectively. The dash lines represented the 95% predictive interval. (For interpretation of the references to color in this figure legend, the reader is referred to the Web version of this article.)

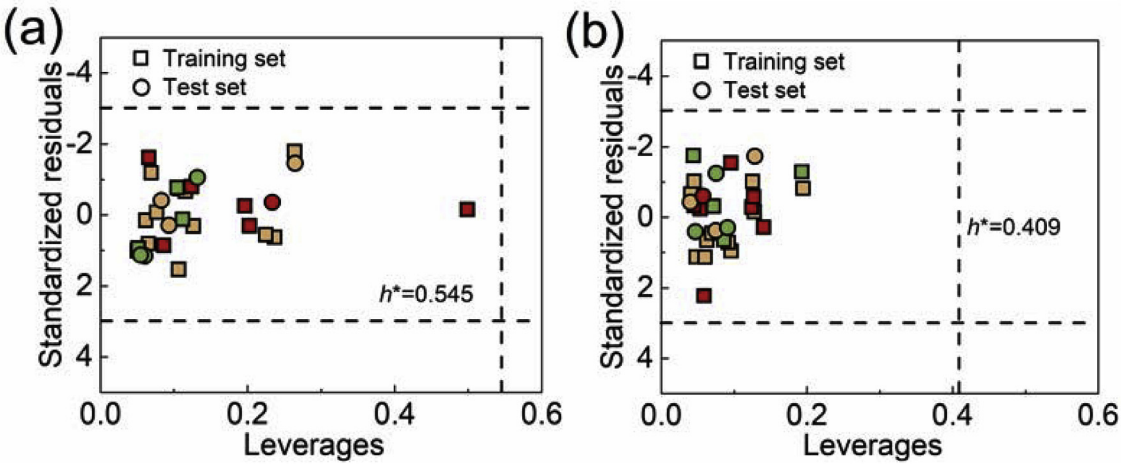

Fig. 3. Williams plots for the QSAR models at (a) pH 7 and (b) pH 10. Fill colors with orange, red, and green were represented for monosubstituted phenols, pharmaceuticals and other organic compounds, respectively. The horizontal dash lines were standardized residual outliers (±3) and vertical dash lines were warning leverages. (For interpretation of the references to color in this figure legend, the reader is referred to the Web version of this article.)

that the ACs with higher f_{min}^{-} have higher lnk_{obs}. Therefore, the susceptibility of ACs towards attack by electrophiles influences the reactivity of oxidized TAML to some extent.

qH^+ describes the hydrogen bond donating and electrostatic attraction ability, deciding the reactive sites of a molecule to be dehydrogenated. ACs at neutral pH with greater net atomic charge on hydrogen atoms may possess higher reactivity toward oxidized TAML, as suggested by the positive coefficient of qH^+. Most ACs with hydroxyl and carboxyl groups have qH^+ value around 0.5 except for diphenhydramine (0.264) and sulfanilamide (0.437) (Fig. S4e). The N–H or C–H bonds in these two drugs do not react with TAML activators easily though the H-abstraction reaction pathway. The qH^+ was also positively correlate to the rate constants of •OH in the established QSAR model (Luo et al., 2017b). Thus qH^+ is considered a general electrostatic descriptor characterizing interactions between oxidants and ACs whether for radical or non-radical oxidation.

The computed electrostatic potential on the molecular surface of two example ACs (4-chlorophenol and BPA) are shown in Fig. 4, in which the blue color represents most positive value while the red color illustrates most negative value. The overall electrostatic potential between 4-chlorophenol and BPA was similar, indicating comparable reactivity with TAML/H_2O_2. Hydrogen atoms (H-13 of 4-chlorophenol, H-18 and H-19 of BPA) in hydroxyl groups have the largest qH^+, and are more easily removed from these compounds. Condensed Fukui indices distribution yield additional insight. The f_{min}^{-} lies in C-5 of 4-chlorophenol and C-19 of BPA, while f_{max}^{-} locates near atoms with f_{min}^{-} (Cl-8 of 4-chlorophenol, C-6 and C-12 of BPA). These regions (atoms with their bonds) indicate the likely reactive sites for attack by oxidized TAML.

The second important descriptor of the pH 10 model is #H:C, which is not included in models at pH 7, indicating a mechanistic difference between the reaction at pH 7 and pH 10. The negative coefficient of #H:C indicates that (at pH 10), ACs with lower ratio of hydrogen atoms to carbon atoms have higher reactivity toward oxidized TAML. This suggests that TAML reacts slowly with the hydrocarbon portion of the molecule and H-abstraction reaction is a crucial step in ACs oxidation. Nevertheless, the correlation between lnk_{obs} and single descriptor #H:C is not significant (Fig. S4d), indicating #H:C should be considered in combination with other factors. #H:C is a simple constitutional descriptor that was not commonly used in previous QSAR models. However, the similar descriptor #O:C exhibited an opposite negative correlation with rate constants for organic contaminants oxidation by $SO_4^{\bullet-}$ (Xiao et al., 2015). A high #O:C ratio means that fewer C–H atoms react by abstracting a hydrogen atom with free $SO_4^{\bullet-}$. Similar results were reported for •OH generated by O_3 for oxidation of organic micropollutants in four river water matrices (Sudhakaran et al., 2012). However, unlike oxidation by TAML/H_2O_2, those are radical-based reactions.

3.3. Hammett correlations

ACs with electron-donating groups are more likely to react

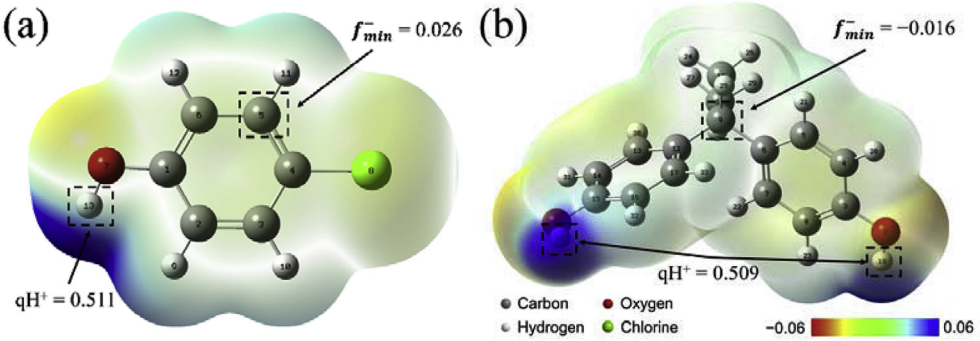

Fig. 4. Computed electrostatic potential on molecular surface of neutral (a) 4-chlorophenol and (b) Bisphenol A.

through the SET pathway than that with electron–withdrawing groups (Luo et al., 2017c). Due to the possible occurrence of the SET pathway for AC oxidation by TAML/H_2O_2, we investigated the influence of electron-donating groups on the relative rate constants k_{rel} ($k_{rel} = k_{obs}/k_{phenol}$) of monosubstituted phenols, using phenol as the reference compound for normalization (Fig. S5). Amino, hydroxyl, and methoxy groups were categorized as strong electron-donating groups, whereas aminoacyl and methyl groups are moderate and weak electron-donating groups, respectively. Halogen, formyl, and nitro groups are weak, moderate, and strong electron-withdrawing groups, respectively (Luo et al., 2017c). As shown in Fig. S5, ln k_{rel} decreases in general from strong electron-donating groups to strong electron-withdrawing groups. However, the relatively low ln k_{rel} value of resorcinol (with meta-hydroxyl group) and high ln k_{rel} value of halogen substituted phenols are in contrast with the trend. This is attributed to different rates of subsequent reaction pathways (e.g. H-abstraction following the SET reaction).

Hammett constants (σ, σ^+ and σ^-) are useful for quantitatively examining the inductive and resonance effect of substituents of ACs especially phenols and anilines on the reaction kinetics (Lee and von Gunten, 2012). The σ^+ and σ^- are particular scopes of σ constants for the electron-donating substituents and the electron-withdrawing substituents, respectively, which have been used for stabilization of reaction centers via resonance interaction with substituents (Lee and von Gunten, 2012). The large negative values of Hammett constants describing electron-donating properties of substituents while electron-withdrawing substituents have positive value. Therefore, Hammett correlations were established between lnk_{obs} of a series of monosubstituted phenols, and the Hammett constants σ, σ^+ and σ^- are listed in Table S7. The rate constants of a series of substituted phenols are negatively correlated to σ and σ^+, but in poor correlation with σ^- (Fig. 5 and Fig. S6). This suggests that the regression equations on Fig. 5a and d with relatively high R^2 (>0.74) are simple for predicting the rate constant (lnk_{obs}) for the oxidation of phenolic contaminants by TAML/H_2O_2, where 25 out of 28 (89.3%) predicted lnk_{obs} are within a factor of 0.5–2. The lnk_{obs} is inversely proportional to Hammett constants, which is typical for electrophilic reactions. These results are consistent with previous studies on the oxidation of phenols and anilines by relevant oxidants (O_3 (Lee and von Gunten, 2012), ClO_2 (Lee and von Gunten, 2012), Fe (VI) (Lee and von Gunten, 2012), bovine methemoglobin (Pérez-Prior et al., 2012), lactoperoxidase (Zhang and Dunford, 1993), and HRP (Na and Lee, 2017)), but are different from oxidation processes with singlet oxygen ($^1O_2$) (Tratnyek and Hoigne, 1991) and MnO_2 (Salter-Blanc et al., 2016), which correlate better with σ^- constants.

The slope (ρ) of the correlation reflects the sensitivity of the reaction to the substituent effect. The lower slope ($\rho = -3.63$ and -1.98 for variables σ and σ^+, respectively) of the pH 7 model compared to that for pH 10 ($\rho = -5.83$ and -3.41 for variables σ and σ^+, respectively) indicates that reaction at pH 7 is less sensitive to the substituent variation. This is consistent with the Hammett relationships based on σ^+ for oxidation kinetics of neutral and deprotonated phenolics by Fe (VI) (Lee and von Gunten, 2012) and potassium permanganate (Mn (VII)) (Song et al., 2015). These observations suggest that the reaction mechanism for TAML/H_2O_2 with phenols at pH 7 is different from that at pH 10. The Hammett correlation between logk_{II} at pH 10 and σ^+ (Fig. S6d) shows that the slope ($\rho = -1.48$) is similar to that of HRP ($\rho = -2.0$) (Na and Lee, 2017). This similar sensitivity to the substituent effect may be due to the comparative reactivity of phenols by enzyme mimic TAML and natural peroxidase.

The lnk_{obs} values of halogenated phenols (4-chlorophenol and 4-bromophenol) are higher than those predicted by Hammett constants, indicating that the reactivity of phenols with TAML/H_2O_2 may not simply follow the Hammett correlations. They were therefore excluded in the linear regression. This is in contrast to the oxidation of chloro- and bromo-substituted BPA by TAML/H_2O_2, which have lower k_{II} than pristine BPA and methyl-substituted BPA (Onundi et al., 2017). It is known that the halogen substituents are weak electron-withdrawing groups that can reduce the electron density of aromatic compounds, making them resistant to chemical or biological oxidation. Nevertheless, TAML/H_2O_2 could completely mineralize chlorophenols through an oxidative ring-opening pathway and the degradation rate increased with an increased number of electron-withdrawing chlorine groups on the phenol ring (initial degradation rate: pentachlorophenol > 2,4,6-trichlorophenol > 2,4-dichlorophenol), which disagrees with the Hammett correlation (Collins et al., 2010; Gupta et al., 2002). A possible reason is that the higher f_{min}^- value of 4-chlorophenol (0.026) and 4-bromophenol (0.025) make them more susceptibly attack by oxidized TAML (Fig. 4a).

The lnk_{obs} of salicylaldehyde is also significantly larger than the QSAR prediction. The ortho-substituted hydroxybenzaldehyde was predicted to have lower lnk_{obs} than the para-substituted compounds, but the opposite result was observed. Similar discrepancies were found for nitrophenol oxidation by TAML activators; 2-nitrophenol has higher k_I (154 M^{-1} s^{-1}) than 4-nitrophenol (k_I = 33 M^{-1} s^{-1}) (Kundu et al., 2015). Note that the 4-nitrophenol is a strong inhibitor of catalytic activity due to steric suppression of reversible binding of nitrophenolate anions to the iron center (Kundu et al., 2015). This suggests that 4-hydroxybenzaldehyde exerts a similar steric effect, thus limiting the value of Hammett correlations.

3.4. The pH-dependent mechanism

Considerable differences between TAML/H_2O_2 oxidation of ACs at neutral and basic pH were observed both in the QSAR models and Hammett correlations. This indicates that the reaction mechanism changes with pH. Furthermore, the rate constants of ACs in our study and previous studies show strong pH-dependent reactions of TAML activators. This pH-dependent feature could be attributed to two possible reasons: (1) The reactive species of oxidized TAML formed by TAML and H_2O_2 were generated faster at pH 10 (higher k_I); (2) the dissociated ACs (most with pKa <10) at pH 10 have a higher electron density and thus are more reactive to electrophilic agents (oxidized TAML). Both effects lead to a significant increase in rate as pH increases from 7 to 10. From Scheme 1, the TAML/H_2O_2 generally form an oxidized TAML then reacts with ACs. These highly reactive species were characterized as high valence iron-oxo complex (Fe^V–O) (De Oliveira et al., 2007) or Fe^{IV}–O (Ghosh et al., 2008) depending on pH. The deprotonated form of TAML with −2 charge has the highest activity to react with H_2O_2 at around pH 10 (Ghosh et al., 2008), and the k_I decreases above pH 10 due to the deprotonation of H_2O_2 (pKa >11), suggesting that the highest reactivity of TAML/H_2O_2 falls in a narrow range between pH 10 and 11.

Our QSAR models helps understand the results of ACs degradation at different pH values. Generally, ACs are rapidly destroyed and toxicity decreases at the optimal pH (Gupta et al., 2002; Shappell et al., 2008), but unintended intermediates may be generated at sub-optimal pH (Chanda et al., 2006b; Onundi et al., 2017; Shen et al., 2011). For example, during BPA oxidation by TAML/H_2O_2, BPA is condensed into oligomers at neutral pH while destroyed to small molecules at pH 11 (Onundi et al., 2017). The initial step of TAML/H_2O_2 oxidative degradation of BPA at neutral pH is SET followed by H-abstraction (Eq. (11), Fig. S7). The primary radical-cation molecules are the precursors of the coupled C–C and C–O dimers. A potential explanation is that the removal of an

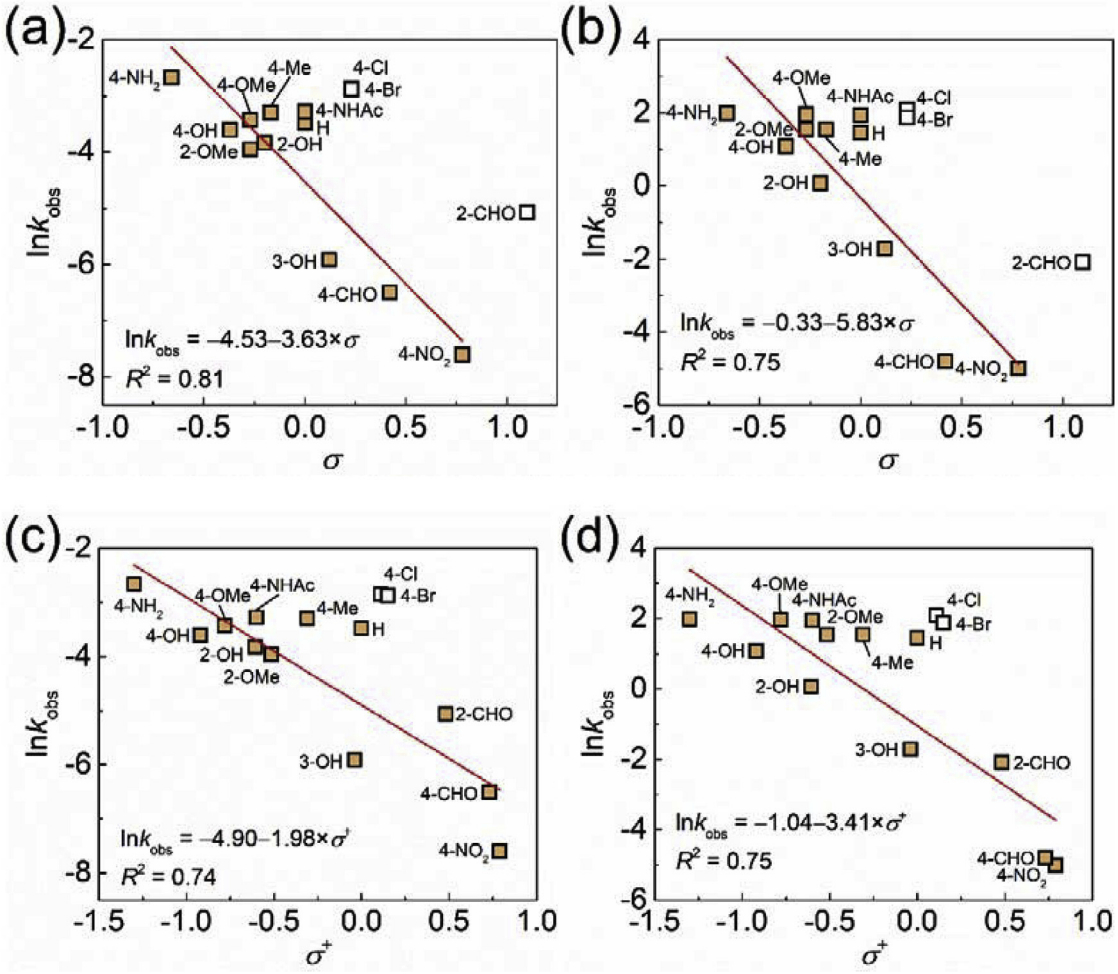

Fig. 5. Correlation between $\ln k_{obs}$ of monosubstituted phenols and Hammett constants σ and σ^+: (a) $\ln k_{obs}$ at pH 7 vs. σ, (b) $\ln k_{obs}$ at pH 10 vs. σ, (c) $\ln k_{obs}$ at pH 7 vs. σ^+, and (d) $\ln k_{obs}$ at pH 10 vs. σ^+. The hollow squares were not included in the linear regressions.

electron from the HOMO of the molecule leads to this pathway, indicating that the SET from the BPA to the oxidized TAML was a rate limiting reaction steps. A hydrogen atom (H-18 or H-19) with higher positive charge (Fig. 4b) is removed subsequently. The oxidative coupling reactions of BPA is in agreement with natural HRP/H_2O_2 systems (Huang and Weber, 2005). For the fast and complete degradation at pH 10, the BPA undergoes SET followed by heterolysis (possibly occurred between C-6 or C-12 and C-19) to form hydroquinone and then destroyed through ring-fission pathways. The possible rate limiting step under this condition is hydrogen atom transfer, thus constitute of total molecule (#H:C) plays a vital role in the oxidation of ACs (Eq. (12)). To summarize, pH-dependent reactivity and degradation pathways yield different QSAR models at neutral and basic pH values, underscoring the importance to consider pH depending mechanism when using TAML/H_2O_2 in wastewater treatment process.

4. Conclusions

We demonstrated rapid TAML/H_2O_2-based oxidation of a broad range of ACs, indicating that this advanced oxidation process had great potential as an efficient approach for water purification. First-order degradation rate constants (k_{obs}) for 29 ACs were determined at pH 7 and pH 10, and were used to develop QSAR models to predict rate constants and inform rate-limiting mechanisms. These models are:

$$\ln k_{obs} = 2.32 + 1.95 \times E_{HOMO} + 11.6 \times qH^+ + 27.9 \times f_{min}^- \text{ at pH 7, and}$$

$$\ln k_{obs} = 35.6 + 4.53 \times E_{HOMO} - 7.42 \times \#H : C \text{ at pH 10.}$$

Accordingly, the reactivity of TAML/H_2O_2 increases with the electron donating ability, and is influenced by the electrostatic distribution and molecular composition of ACs. Hammett constants are simple but not accurate predictors of rate constants for phenolic compounds. Different reaction pathways may occur for some ACs under various pH values, as is the case for natural enzymes. These models could be used as a prescreening tool to identify which ACs could be efficiently oxidized, and provide novel insight on pH-dependent degradation mechanism for such non-radical mediated advanced oxidation processes. The high efficiency of TAML-based treatment simulated by our QSAR model is based on parameters determined under laboratory conditions. This model could also apply to organic contaminants oxidation in complex wastewater matrices. However, this would require determining system-specific rate constants for the TAML/H_2O_2 system in the presence of potentially interfering constituents (e.g., natural organic matters, ions, and alkalinity) for accurate assessments of reaction rates under complex environmental conditions.

Acknowledgements

Financial supports from Shanghai Municipal International Cooperation Foundation (No. 15230724600), Special Fund for Agro-scientific Research in the Public Interest (201503107) and the NSF ERC on Nanotechnology-Enabled Water Treatment (EEC-1449500) are gratefully acknowledged.

Appendix A. Supplementary data

Supplementary data related to this article can be found at https://doi.org/10.1016/j.watres.2018.04.062.

References

Borhani, T.N.G., Saniedanesh, M., Bagheri, M., Lim, J.S., 2016. QSPR prediction of the hydroxyl radical rate constant of water contaminants. Water Res. 98, 344–353.
Chahbane, N., Popescu, D., Mitchell, D.A., Chanda, A., Lenoir, D., Ryabov, A.D., Schramm, K., Collins, T.J., 2007. Fe^{III}-TAML-catalyzed green oxidative degradation of the azo dye Orange II by H_2O_2 and organic peroxides: products, toxicity, kinetics, and mechanisms. Green Chem. 9 (1), 49–57.
Chanda, A., Ryabov, A.D., Mondal, S., Alexandrova, L., Ghosh, A., Hangun-Balkir, Y., Horwitz, C.P., Collins, T.J., 2006a. Activity-stability parameterization of homogeneous green oxidation catalysts. Chem. Eur J. 12 (36), 9336–9345.
Chanda, A., Khetan, S.K., Banerjee, D., Ghosh, A., Collins, T.J., 2006b. Total degradation of fenitrothion and other organophosphorus pesticides by catalytic oxidation employing Fe-TAML peroxide activators. J. Am. Chem. Soc. 128 (37), 12058–12059.
Chen, J.L., Ravindran, S., Swift, S., Wright, L.J., Singhal, N., 2012. Catalytic oxidative degradation of 17α-ethinylestradiol by Fe^{III}-TAML/H_2O_2: estrogenicities of the products of partial, and extensive oxidation. Water Res. 46 (19), 6309–6318.
Collins, T.J., Khetan, S.K., Ryabov, A.D., 2010. Chemistry and applications of Iron–TAML catalysts in green oxidation processes based on hydrogen peroxide. In: Handbook of Green Chemistry. Wiley-VCH Verlag GmbH & Co. KGaA, pp. 39–77.
De Oliveira, F.T., Chanda, A., Banerjee, D., Shan, X., Mondal Jr., S., Que, L., Bominaar, E.L., Muenck, E., Collins, T.J., 2007. Chemical and spectroscopic evidence for an Fe-V-Oxo complex. Science 315 (5813), 835–838.
Ellis, W.C., Tran, C.T., Denardo, M.A., Fischer, A., Ryabov, A.D., Collins, T.J., 2009. Design of more powerful Iron-TAML peroxidase enzyme mimics. J. Am. Chem. Soc. 131 (50), 18052–18053.
Ellis, W.C., Tran, C.T., Roy, R., Rusten, M., Fischer, A., Ryabov, A.D., Blumberg, B., Collins, T.J., 2010. Designing green oxidation catalysts for purifying environmental waters. J. Am. Chem. Soc. 132 (28), 9774–9781.
Ghosh, A., Ryabov, A.D., Mayer, S.M., Horner, D.C., Prasuhn, D.E., Sen Gupta, S., Vuocolo, L., Culver, C., Hendrich, M.P., Rickard, C.E.F., Norman, R.E., Horwitz, C.P., Collins, T.J., 2003. Understanding the mechanism of H^+-Induced demetalation as a design strategy for robust iron(III) peroxide-activating catalysts. J. Am. Chem. Soc. 125 (41), 12378–12379.
Ghosh, A., Mitchell, D.A., Chanda, A., Ryabov, A.D., Popescu, D.L., Upham, E.C., Collins, G.J., Collins, T.J., 2008. Catalase–peroxidase activity of Iron(III)–TAML activators of hydrogen peroxide. J. Am. Chem. Soc. 130 (45), 15116–15126.
Gupta, S.S., Stadler, M., Noser, C.A., Ghosh, A., Steinhoff, B., Lenoir, D., Horwitz, C.P., Schramm, K.W., Collins, T.J., 2002. Rapid total destruction of chlorophenols by activated hydrogen peroxide. Science 296 (5566), 326–328.
Hu, P., Su, H., Chen, Z., Yu, C., Li, Q., Zhou, B., Alvarez, P.J.J., Long, M., 2017. Selective degradation of organic pollutants using an efficient metal-free catalyst derived from carbonized polypyrrole via peroxymonosulfate activation. Environ. Sci. Technol. 51 (19), 11288–11296.
Huang, Q., Weber, W.J., 2005. Transformation and removal of bisphenol A from aqueous phase via peroxidase-mediated oxidative coupling reactions: efficacy, products, and pathways. Environ. Sci. Technol. 39 (16), 6029–6036.
Kundu, S., Chanda, A., Thompson, J.V.K., Diabes, G., Khetan, S.K., Ryabov, A.D., Collins, T.J., 2015. Rapid degradation of oxidation resistant nitrophenols by TAML activator and H_2O_2. Catal. Sci. Technol. 5 (3), 1775–1782.
Lee, M., Zimmermann-Steffens, S.G., Arey, J.S., Fenner, K., von Gunten, U., 2015. Development of prediction models for the reactivity of organic compounds with ozone in aqueous solution by quantum chemical calculations: the role of delocalized and localized molecular orbitals. Environ. Sci. Technol. 49 (16), 9925–9935.
Lee, Y., von Gunten, U., 2012. Quantitative structure–activity relationships (QSARs) for the transformation of organic micropollutants during oxidative water treatment. Water Res. 46 (19), 6177–6195.
Luo, S., Wei, Z., Spinney, R., Yang, Z., Chai, L., Xiao, R., 2017a. A novel model to predict gas–phase hydroxyl radical oxidation kinetics of polychlorinated compounds. Chemosphere 172, 333–340.
Luo, X., Yang, X., Qiao, X., Wang, Y., Chen, J., Wei, X., Peijnenburg, W.J.G.M., 2017b. Development of a QSAR model for predicting aqueous reaction rate constants of organic chemicals with hydroxyl radicals. Environ. Sci. Proc. Impacts 19 (3), 350–356.
Luo, S., Wei, Z., Dionysiou, D.D., Spinney, R., Hu, W., Chai, L., Yang, Z., Ye, T., Xiao, R., 2017c. Mechanistic insight into reactivity of sulfate radical with aromatic contaminants through single-electron transfer pathway. Chem. Eng. J. 327, 1056–1065.
Luo, S., Wei, Z., Spinney, R., Zhang, Z., Dionysiou, D.D., Gao, L., Chai, L., Wang, D., Xiao, R., 2018a. UV direct photolysis of sulfamethoxazole and ibuprofen: an experimental and modelling study. J. Hazard Mater. 343, 132–139.
Luo, S., Wei, Z., Spinney, R., Villamena, F.A., Dionysiou, D.D., Chen, D., Tang, C., Chai, L., Xiao, R., 2018b. Quantitative structure-activity relationships for reactivities of sulfate and hydroxyl radicals with aromatic contaminants through single-electron transfer pathway. J. Hazard Mater. 344, 1165–1173.
Na, S., Lee, Y., 2017. Elimination of trace organic contaminants during enhanced wastewater treatment with horseradish peroxidase/hydrogen peroxide (HRP/H_2O_2) catalytic process. Catal. Today 282, 86–94.
Onundi, Y., Drake, B.A., Malecky, R.T., DeNardo, M.A., Mills, M.R., Kundu, S., Ryabov, A.D., Beach, E.S., Horwitz, C.P., Simonich, M.T., Truong, L., Tanguay, R.L., Wright, L.J., Singhal, N., Collins, T.J., 2017. A multidisciplinary investigation of the technical and environmental performances of TAML/peroxide elimination of bisphenol A compounds from water. Green Chem. 19 (18), 4234–4262.
Pal, A., Gin, K.Y., Lin, A.Y., Reinhard, M., 2010. Impacts of emerging organic contaminants on freshwater resources: review of recent occurrences, sources, fate and effects. Sci. Total Environ. 408 (24), 6062–6069.
Pérez-Prior, M.T., Gómez-Bombarelli, R., González-Sánchez, M.I., Valero, E., 2012. Biocatalytic oxidation of phenolic compounds by bovine methemoglobin in the presence of H_2O_2: quantitative structure–activity relationships. J. Hazard Mater. 241–242, 207–215.
Ponder, J.W., 2004. Tinker: Software Tools for Molecular Design. Version 5.1.9. https://dasher.wustl.edu/tinker/.
Radian, A., Fichman, M., Mishael, Y., 2015. Modeling binding of organic pollutants to a clay–polycation adsorbent using quantitative structural–activity relationships (QSARs). Appl. Clay Sci. 116–117, 241–247.
Sakurada, J., Sekiguchi, R., Sato, K., Hosoya, T., 1990. Kinetic and molecular orbital studies on the rate of oxidation of monosubstituted phenols and anilines by horseradish peroxidase compound II. Biochemistry 29 (17), 4093–4098.
Salter-Blanc, A.J., Bylaska, E.J., Lyon, M.A., Ness, S.C., Tratnyek, P.G., 2016. Structure–activity relationships for rates of aromatic amine oxidation by manganese dioxide. Environ. Sci. Technol. 50 (10), 5094–5102.
Shappell, N.W., Vrabel, M.A., Madsen, P.J., Harrington, G., Billey, L.O., Hakk, H., Larsen, G.L., Beach, E.S., Horwitz, C.P., Ro, K., Hunt, P.G., Collins, T.J., 2008. Destruction of estrogens using Fe-TAML/peroxide catalysis. Environ. Sci. Technol. 42 (4), 1296–1300.
Shen, L.Q., Beach, E.S., Xiang, Y., Tshudy, D.J., Khanina, N., Horwitz, C.P., Bier, M.E., Collins, T.J., 2011. Rapid, biomimetic degradation in water of the persistent drug sertraline by TAML catalysts and hydrogen peroxide. Environ. Sci. Technol. 45 (18), 7882–7887.
Song, Y., Jiang, J., Ma, J., Pang, S., Liu, Y., Yang, Y., Luo, C., Zhang, J., Gu, J., Qin, W., 2015. ABTS as an electron shuttle to enhance the oxidation kinetics of substituted phenols by aqueous permanganate. Environ. Sci. Technol. 49 (19), 11764–11771.
Sudhakaran, S., Amy, G.L., 2013. QSAR models for oxidation of organic micropollutants in water based on ozone and hydroxyl radical rate constants and their chemical classification. Water Res. 47 (3), 1111–1122.
Sudhakaran, S., Calvin, J., Amy, G.L., 2012. QSAR models for the removal of organic micropollutants in four different river water matrices. Chemosphere 87 (2), 144–150.
Tang, L.L., DeNardo, M.A., Gayathri, C., Gil, R.R., Kanda, R., Collins, T.J., 2016. TAML/H_2O_2 oxidative degradation of metaldehyde: pursuing better water treatment for the most persistent pollutants. Environ. Sci. Technol. 50 (10), 5261–5268.
Tratnyek, P.G., Hoigne, J., 1991. Oxidation of substituted phenols in the environment: a QSAR analysis of rate constants for reaction with singlet oxygen. Environ. Sci. Technol. 25 (9), 1596–1604.
Tropsha, A., Gramatica, P., Gombar, V.K., 2003. The importance of being earnest: validation is the absolute essential for successful application and interpretation of QSPR models. QSAR Comb. Sci. 22 (1), 69–77.
Wang, C., Gao, J., Gu, C., 2017a. Rapid destruction of tetrabromobisphenol A by iron(III)-tetraamidomacrocyclic ligand/layered double hydroxide composite/H_2O_2 system. Environ. Sci. Technol. 51 (1), 488–496.
Wang, R., Bai, J., Li, Y., Zeng, Q., Li, J., Zhou, B., 2017b. $BiVO_4$/TiO_2(N_2) nanotubes heterojunction photoanode for highly efficient photoelectrocatalytic applications. Nano Micro Lett. 9 (2), 14.
Xiao, R., Ye, T., Wei, Z., Luo, S., Yang, Z., Spinney, R., 2015. Quantitative structure–activity relationship (QSAR) for the oxidation of trace organic contaminants by sulfate radical. Environ. Sci. Technol. 49 (22), 13394–13402.
Xiao, R., Gao, L., Wei, Z., Spinney, R., Luo, S., Wang, D., Dionysiou, D.D., Tang, C.J., Yang, W., 2017. Mechanistic insight into degradation of endocrine disrupting chemical by hydroxyl radical: an experimental and theoretical approach. Environ. Pollut. 231, 1446–1452.
Xiao, Y., Zhang, L., Zhang, W., Lim, K., Webster, R.D., Lim, T., 2016. Comparative evaluation of iodoacids removal by UV/persulfate and UV/H_2O_2 processes. Water Res. 102, 629–639.
Yang, W., Mortier, W.J., 1986. The use of global and local molecular parameters for the analysis of the gas-phase basicity of amines. J. Am. Chem. Soc. 108 (19), 5708–5711.
Yang, Z., Luo, S., Wei, Z., Ye, T., Spinney, R., Chen, D., Xiao, R., 2016. Rate constants of hydroxyl radical oxidation of polychlorinated biphenyls in the gas phase: a

single–descriptor based QSAR and DFT study. Environ. Pollut. 211, 157–164.
Ye, T., Wei, Z., Spinney, R., Dionysiou, D.D., Luo, S., Chai, L., Yang, Z., Xiao, R., 2017. Quantitative structure-activity relationship for the apparent rate constants of aromatic contaminants oxidized by ferrate (VI). Chem. Eng. J. 317, 258–266.
Zhan, C., Nichols, J.A., Dixon, D.A., 2003. Ionization potential, electron affinity, electronegativity, hardness, and electron excitation energy: molecular properties from density functional theory orbital energies. J. Phys. Chem. A 107 (20), 4184–4195.
Zhang, H., Dunford, H.B., 1993. Hammett pσ correlation for reactions of lactoperoxidase compound II with phenols. Can. J. Chem. 71 (12).
Zheng, L., Yu, X., Long, M., Li, Q., 2017. Humic acid mediated visible light degradation of phenol on the phosphate and Nafion modified TiO_2 surface. Chin. J. Catal. 38 (12), 2076–2084.
Zhu, H., Guo, W., Shen, Z., Tang, Q., Ji, W., Jia, L., 2015. QSAR models for degradation of organic pollutants in ozonation process under acidic condition. Chemosphere 119, 65–71.